Materials Science in Semiconductor Processing 165 (2023) 107693

Contents lists available at ScienceDirect

Materials Science in Semiconductor Processing

journal homepage: www.elsevier.com/locate/mssp

MBE-based growth of Sn-rich quantum wells and dots at low Sn deposition rates

Ahsan Hayat [a], Davide Spirito [b], Agnieszka Anna Corley-Wiciak [b], Markus Andreas Schubert [b], Maria Masood [b], Felix Reichmann [b], Markus Ratzke [a], Giovanni Capellini [b,c], Inga Anita Fischer [a,*]

[a] Experimental Physics and Functional Materials, BTU Cottbus–Senftenberg, Cottbus, Germany
[b] IHP—Leibniz-Institut für innovative Mikroelektronik, Frankfurt (Oder), Germany
[c] Dipartimento di Scienze, Universita degli Studi Roma Tre, Rome, Italy

ARTICLE INFO

Keywords:
MBE growth
GeSn
Quantum island growth
Photoluminescence spectra

ABSTRACT

Alloying Ge with Sn is a possible route towards obtaining a direct bandgap material that can be integrated with Si technology for optoelectronic device applications. Low-dimensional structures such as GeSn quantum wells or islands are of particular interest, since those applications can benefit from quantum confinement effects. Here, we investigate the formation of Sn-rich quantum wells and islands formed by the deposition of few MLs of Sn on Ge and their overgrowth with Ge both based on a morphological characterization of the samples as well as photoluminescence measurements. We find that a low substrate temperature as well as a low deposition rate have an impact on the critical layer thickness at which the onset of Sn island formation can be observed and discuss the implications both for the samples grown and future research efforts.

1. Introduction

Si-based photonics is under the spotlight in both applied and fundamental research thanks to its unique toolbox comprising on-chip detectors, modulators, and light sources for applications in e.g. data transmission, imaging, and sensing [1]. While photodetectors based on Ge have reached the performances and the technology level to be manufactured in semiconductor foundries running on qualified CMOS-processes [2,3], to date, a commercial on-chip laser light source directly integrated on a Si wafer remains elusive. In recent years, efforts in realizing light sources based on GeSn alloys that can be potentially integrated on Si have been crowned by some notable success [4]. Very recently, Buca et al. have demonstrated an optically pumped GeSn laser in which the use of a SiN stressor enables the laser emission up to room temperature [5]. Furthermore, the same material has been used in the fabrication of electrically-pumped, microring lasers operating above the liquid nitrogen temperature [6].

The $Ge_{1-y}Sn_y$ has been selected as active material since these alloys have the unique characteristics to have a direct bandgap for a Sn content y in excess of $y \sim 0.08$ when the material is in its diamond lattice, free of any strain possibly arising from its grown on a substrate [7,8]. Indeed, the deposition of $Ge_{1-y}Sn_y$ alloys on Si substrates is extremely challenging owing to the large lattice mismatch of Sn with Si (approx. 20%). For this reason, an intermediate Ge/Si virtual substrate is interposed to partially reduce the lattice mismatch between epilayer and substrate to approx. 14%. Furthermore, Sn has a low solid solubility in Ge (~1% at thermodynamic equilibrium [9]) and, consequently, out-of-equilibrium deposition processes had to be developed to incorporate a Sn content of interest for optoelectronic applications, while avoiding Sn segregation [10].

In this context, low dimensional GeSn structures such as quantum wells (QW) [11–13] and quantum dots (QD) [14–18] have been investigated. They are also of interest for the concomitant quantum confinement effects that could positively impact the radiative recombination processes, and the impact of QW on optoelectronic device performance has been demonstrated [19–21].

One strategy for the growth of $Ge_{1-y}Sn_y$ QW and QD with large Sn content is the deposition of pure Sn layers and their overgrowth with Ge using molecular beam epitaxy (MBE) [18,22–26]. Indeed, the deposition of few MLs of pure Sn on Ge follows Stranski-Krastanov growth, similarly to the growth of pure Ge on Si [27]. In the initial stage, a continuous wetting layer (WL) is formed. The WL lattice is coherent to the

* Corresponding author.
E-mail address: inga.fischer@b-tu.de (I.A. Fischer).

https://doi.org/10.1016/j.mssp.2023.107693
Received 26 December 2022; Received in revised form 20 April 2023; Accepted 22 June 2023
Available online 28 June 2023
1369-8001/© 2023 The Authors. Published by Elsevier Ltd. This is an open access article under the CC BY license (http://creativecommons.org/licenses/by/4.0/).

underlying lattice and elastic energy is therefore accumulated until a certain critical thickness h_c is reached. Beyond h_c, the additional deposition of Sn leads to the strain relaxation of the epi-layer via the formation of three dimensional islands. This onset of island growth has previously been reported to be $h_c = 2.25$ MLs [28].

The intermixing of Sn and Ge at the heterointerface [29] and the segregation of Sn could potentially influence the compositional profile along the growth direction, as it was observed in the case of the deposition of ~2 MLs of pure Sn followed by an overgrowth with Ge, which resulted in the formation of multiple-QW made of a GeSn well featuring a maximum Sn content of ~15% surrounded by Ge barriers [26]. However, the resulting QW were so thin that the alloys optical transitions were of indirect nature, owing to the higher confinement energy of the Γ-valley electrons as compared to those in the L-valley, prevailing against the effect of the Sn presence on the "directness" of the electron energy landscape.

This suggests that, in order to harness the benefits of such Sn-rich QWs and QDs for optoelectronic device applications, a strong focus should be put on increasing the thickness of the Sn-rich regions, both by increasing the WL thickness and by exceeding h_c and reaching the initial stages of QD growth. In the latter case, the incorporation of the Sn-rich QD into a Ge matrix, also has to be thoroughly investigated.

Within this framework, here we report on the investigation of wetting layer formation and Sn-rich island growth using MBE at a substrate temperature of 60 °C and a Sn deposition rate of $r_{Sn} = 0.013$ Å/s. In this growth regime, we find that WL thicknesses as large as 4 ML can be reached before large islands form. Our photoluminescence measurement results indicate that, despite the larger thickness of the quantum wells compared to earlier investigations, indirect transitions still dominate. Our results, however, demonstrate that reducing both substrate temperature and Sn deposition rate has a positive impact on the thickness of the Sn-rich regions in our structures and, thus, provides a starting point for growth strategies for the fabrication of Sn-rich quantum islands and wells in which direct transitions can be harnessed for applications in optoelectronic devices.

2. Material growth and characterization methods

In our research work, four different samples were fabricated on a Ge/Si (001) virtual substrate (VS) using molecular beam epitaxy (MBE) at low substrate temperatures. The Ge/Si (001) VS was realized by depositing using a CVD-based process a fully relaxed, 2 μm thick Ge epilayer on Si (001) 200 mm wafers (see Ref. [30] for details). Prior to MBE growth, the Ge/Si (001) wafers were cut into 7 × 7 mm^2 pieces, loaded into the ultra-high vacuum, degassed at around 700 °C for 10 min, and subsequently cleaned by three cycles of argon sputtering with 500 eV energy and annealed at about 150 °C for 3 min. Prior to the deposition of Sn, approx. 10 nm of Ge were deposited in order to obtain a pristine surface for high quality growth. In our work, two samples of uncapped Sn dots and Sn dots capped with Ge were fabricated on the 7 × 7 mm^2 substrates (Table 1, see also Fig. 1). For Sn deposition, a Focus EFM-3 Evaporator was used at sample temperatures of 60 °C and pre-calibrated for a Sn deposition rate of $r_{Sn} = 0.013$ Å/s. Sample temperatures were measured using a thermocouple attached to the sample manipulator. The Sn deposition time was selected to be 9 min, (4.4 ML of Sn corresponding to 0.7 nm), and, 15 min, (7.4 ML, i.e. 1.2 nm), respectively. In the case of the capped samples, the Sn layer was immediately overgrown with a ~30 nm-thick Ge cap layer using a Createc effusion cell (cell temperature was maintained at 1200 °C, deposition time 15 min).

Table 1
Sample overview.

Name	Sn deposited (ML)	Ge cap thickness (nm)
Sample A	4.4 (0.7 nm)	0
Sample B	7.4 (1.2 nm)	0
Sample C	4.4 (0.7 nm)	30
Sample D	7.4 (1.2 nm)	30

The morphology of the uncapped samples was characterized using atomic force microscopy (AFM) in tapping mode (Dimension Icon with the NanoScope V controller equipped with 90 μm × 90 μm × 6 μm XYZ scanner, Bruker, Billerica, MA, USA). The morphology and atomic structure of the capped samples were investigated via cross-sectional images obtained from transmission electron microscopy in the STEM (scanning transmission electron microscopy) and HRTEM (high-resolution transmission electron microscopy) regimes on a Tecnai Osiris, electron microscope (FEI) at the accelerating voltage of 200 kV. For HRTEM studies, the samples were prepared as transverse slices (1 1 0) using an optimized technique, including the grinding, polishing, and small-angle ion etching initially at the ion beam energies of 6 keV and then reducing the ion beam energies to 2.5 keV in the thinning stage. The digital processing of experimental HRTEM images was carried out using the commercial software package GMS-1.8 (GATAN).

Optical characterization of the capped samples was carried out using a Macro-photoluminescence (Macro-PL) measurement setup at lattice temperatures varying between 13 and 80 K in a custom-designed Horiba setup, a high-resolution spectrometer optimized for IR measurements (Horiba iHR320), and a single channel extended-InGaAs detector (0.496–1.1 eV detection range). A 1064 nm laser with an output optical power density at the sample in the 0.3 - 2.0 W/cm^2 range was used, incident at 45° from the normal on the sample. A parabolic mirror collected the emitted light. A white-body lamp was used to determine the optical response of the setup used for the calibration.

3. Results and discussion

The fabrication of uncapped and capped samples allows us to obtain information on the morphology of the Sn-rich islands before and after the deposition of a cap layer. We now discuss the morphology of the Sn islands by analyzing the AFM measurements acquired on the uncapped samples (A and B). In Fig. 2 we can observe the appearance of three

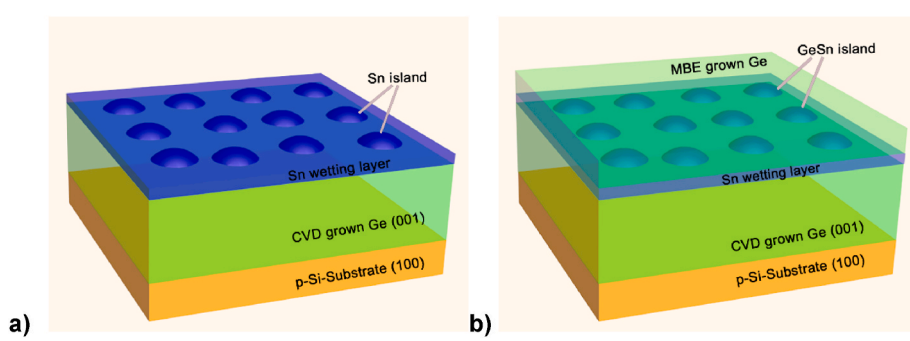

Fig. 1. (a) Schematic view of uncapped Sn-rich islands grown on a Ge/Si (100) substrate by molecular beam epitaxy (b) Schematic view of the Ge-capped Sn islands.

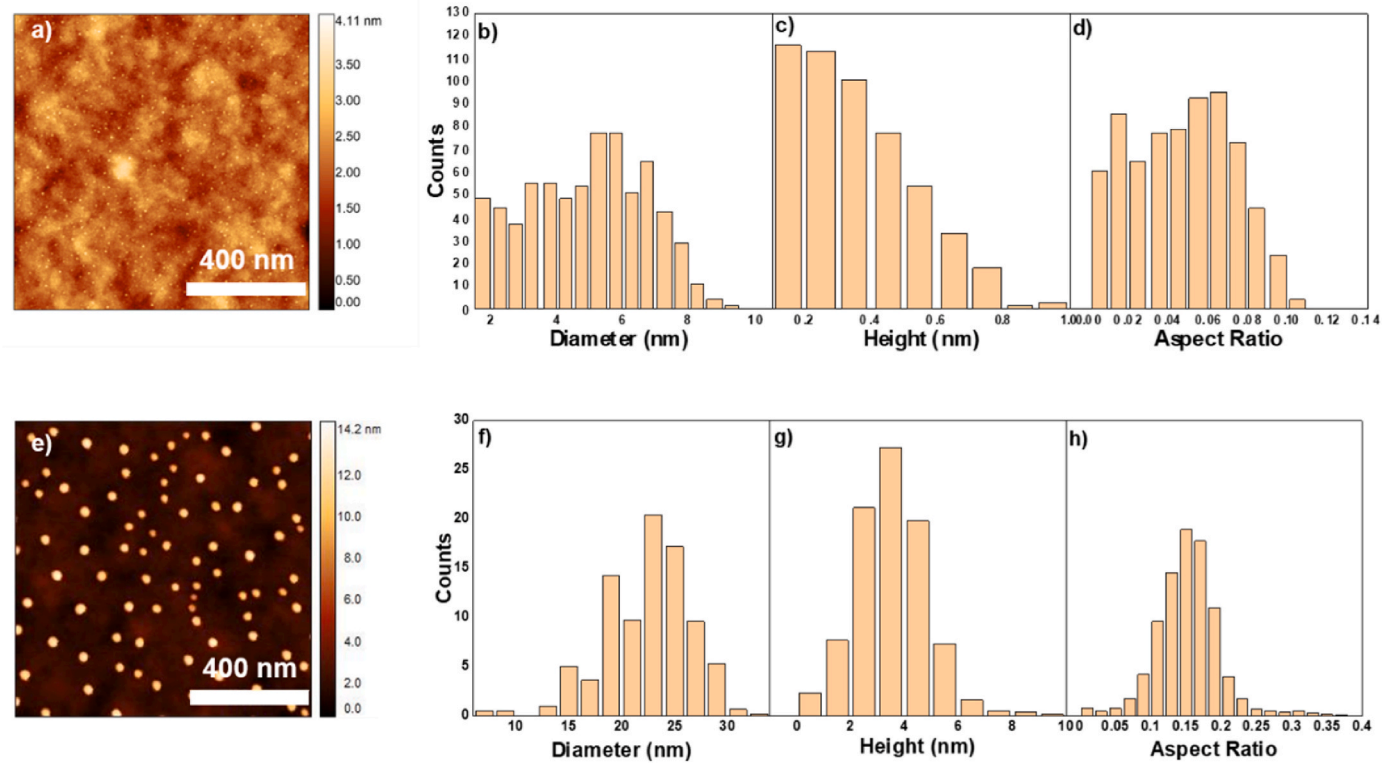

Fig. 2. a) AFM image (1 x 1 μm^2) of Sample A at the onset of Sn-rich island formation as can be seen from the histograms of b) diameters, c) heights and d) aspect ratios of the dots. The 1 x 1 μm^2 AFM image e) of Sample B shows the presence of much larger dots, with histograms of f) diameters, g) heights and h) aspect ratios that have Gaussian shapes.

dimensional clusters on top of both samples. However, the different thicknesses of the deposited Sn layers result in strongly different island morphologies. For Sample A (4.4 ML of Sn), we can see the onset of island formation over the smoother background of the WL surface, with a high surface density of dots that are, on average, only 1 nm in height. On the contrary, Sample B's (7.4 ML of Sn) surface features a lesser density of dots having larger volumes. This is in agreement with previous studies carried out on the Ge/Si system, where the growth dynamics was characterized by a reduction of the island density and increased island size as the deposited material increased [31]. This can be quantified in the histograms of the diameters and the heights of the islands for the two different samples (Fig. 2).

As Fig. 2 b) and c) show, the histogram of heights for Sample A exhibits no clear peak, and aspect ratios (height vs. diameter h/d) of the islands are extremely small. This indicates that the amount of Sn deposited marks the very onset of island formation, i.e. in our growth regime, h_c is only slightly below 4.4 ML. By contrast, the histograms of diameters, heights and aspect ratios of the Sn-rich islands present in Sample B show peaks, with diameters d centered around ~22 nm, heights h centered around 3-4 nm and aspect ratios (h/d) centered around 0.15.

For Samples C and D the deposition of a Ge capping should entail a Sn material redistribution driven by the interdiffusion and the minimization of the heteroepitaxial strain, in the so-called reverse Stranski

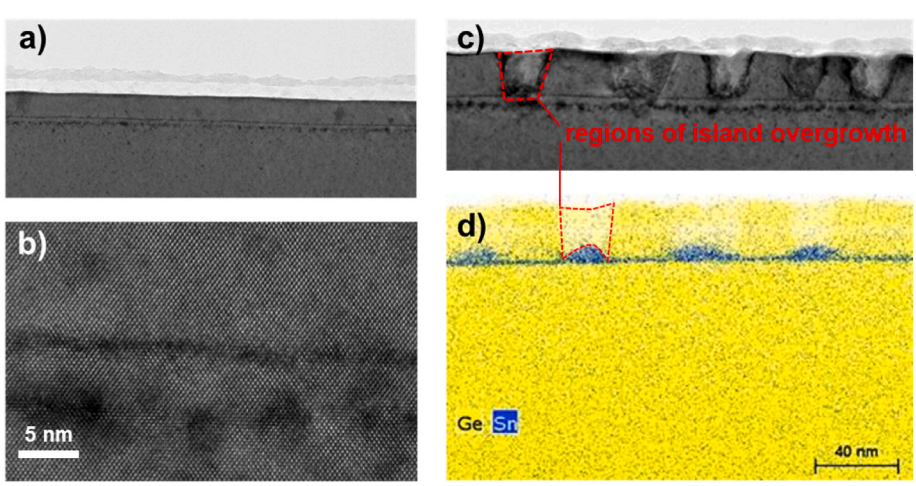

Fig. 3. a) TEM and b) HRTEM cross sectional images of Sample C. The presence of the Sn-rich layer can be seen as a thin line. c) TEM and d) EDX cross sectional images of Sample D. The presence of a Sn-rich wetting layer as well as Sn-rich islands can be clearly seen in the EDX image, however, overgrowth with crystalline Ge can only be observed above the wetting layer. Two representative regions with structural changes in the Ge on top of Sn-rich islands are highlighted in red.

Krastanov transition already observed in the Ge-Si system [32–36].

To assess these capping-induced changes as well as obtain qualitative information on the crystal quality after overgrowth we investigated samples C and D using cross sectional STEM (see Fig. 3). In the cross section of Sample C (4.4 ML of Sn), we can clearly identify a very thin (1.5 – 2 nm) contrast line stemming from the Sn-rich wetting layer. In previous investigations [26], the intermixing of Ge from the substrate with Sn during Sn deposition as well as Sn segregation during overgrowth with Ge was observed to result in a wetting layer composed of a Sn-rich alloy with position-dependent Sn concentration – we assume this to be the case also for Sample C. We could not observe any Sn-rich islands in this sample. This could be attributed to the sparse density of the island observed in the AFM resulting in their absence in the rather thin lamella extracted for the observation, but we argue that this is not the case since an even sparser island population can be detected in sample D, as we shall discuss later. We attribute the "disappearance" of the small clusters observed in the AFM of the corresponding sample A to the effect of the Ge overgrowth resulting in the redistribution of Sn, essentially flattening the islands and getting a "QW" slightly thicker than the WL, typical of the above-mentioned reverse Stranski-Krastanov growth dynamics.

In Sample D (7.4 ML of Sn), the presence of a wetting layer as well as of Sn islands can clearly be seen in the cross-sectional EDX image (Fig. 3 d)). Interestingly, while crystalline Ge can be observed on the top of the Sn-rich wetting layer, structural changes in the material in the regions of island overgrowth as highlighted in red in Fig. 3 c) and 3 d) indicate that island overgrowth with crystalline material, which should have resulted in a cap layer that covers the islands as a continuous blanket, failed. In the case of Ge islands overgrown with Si, different scenarios have been reported in the literature: Epitaxial breakdown can result in the formation of poly-Si/a-Si on top of the islands, which is accompanied by the formation of visible mounds of material on top of the islands [37]. Depending on the growth regime, a formation of dips rather than mounds on top of the islands was also reported during overgrowth [38]. This can be explained by material transport outwards from the islands as mechanism for strain relief. In our case, the large aspect ratios extracted from AFM measurements of the uncapped Sample B indicate that considerable strain relaxation has taken place in the Sn-rich islands in our samples containing 7.4 ML of Sn. In the absence of more detailed simulations of the strain distribution in the Sn-rich islands, a quantitative evaluation of strain relaxation is difficult. Quantitative relationships between aspect ratio and strain relaxation have been extracted based on FEM simulations [39] and measurements [40,41] for Ge islands on Si. An aspect ratio of h/d = 0.15 has been demonstrated to lead to a strain relaxation with $f^* = \frac{a_{Ge}-a_{isl}}{a_{Ge}} \approx 0.45\,\varepsilon$ for Ge islands on Si, where a_{isl} is defined as the lattice constant inside the island, a_{Ge} is the lattice constant of relaxed Ge, and ε is the nominal lattice mismatch between Ge and Si [41]. Because of the lower bulk modulus of α-Sn (0.53 Pa) compared to Ge (0.75 Pa) we take the ratio of $f^*/\varepsilon = 0.45$ as an upper bound for Sn islands on Ge. In the case of continuous layer growth, for the deposition of $Ge_{0.8}Sn_{0.2}$ layers on Ge, epitaxial breakdown has been reported at a critical layer thickness as low as 3 nm [42]. In our case, the surface of sample D does not show the presence of mounds on top of the islands (Fig. 3 c)) and the region of overgrowth appears as yellow interspersed with white, indicating a reduction in atomic density in the thin lamella used for EDX analysis (Fig. 3 d)). We, therefore, argue that the large strain relaxation present in the islands and, as a consequence, the large strain in the Ge cap layer during overgrowth, results in material transport outwards from the islands during overgrowth, creating a region of reduced growth on top of the islands.

Subsequent detailed optical characterizations obtained by PL measurements were carried out on Sample C with 4.4 ML of Sn. Here, based on the cross-sectional TEM images, we assume that the sample contains a laterally homogeneous Sn-rich wetting layer rather than islands as a result of the overgrowth with Ge.

Photoluminescence measurements were obtained for different sample temperatures (Fig. 4 a)) as well as for different excitation power densities (Fig. 4 d)). All spectra can be fitted with two Gaussian peaks, the peak energies as well as their separation are plotted in Fig. 4 b), c) and e), f) with error bars obtained from the fitting procedure. For the series of measurements with different sample temperatures at fixed excitation density, the peak positions vary as a function of temperature (Fig. 4 b)) while the peak separation remains approximately constant (Fig. 4 c). At a lattice temperature of 30 K, the higher energy peak is centered at 527 meV, while the lower energy peak is centered at 510 meV – both transition energies are noticeably lower than for samples with a WL thickness of 2 ML at the same lattice temperature, where a transition energy of 546 meV was observed [26]. This is a consequence of the larger thickness of the Sn-rich region attained in our sample. The decrease of peak energy with increasing temperature in our sample (Fig. 4 b)) can be explained by the reduction in band gap with increasing temperature as described by Varshni's law. The fact that the peak separation remains approximately constant strongly indicates that the optical transitions in the material remain indirect, with the Gaussian peak at lower energies originating from phonon-assisted transitions, and the Gaussian peak at higher energies originating from no-phonon transitions. In the case of no-phonon transitions, impurities can serve to supply the momentum difference for radiative recombination. In the case of phonon-assisted transitions, the peak separation of ~15 meV can be assigned to the energy of the phonons involved in order to satisfy momentum conservation. In the absence of detailed information on the position-dependent composition of the Sn-rich wells, we cannot make detailed predictions of the various phonon energies in the Sn-rich layer. We can, however, compare with phonon-assisted optical recombination processes in Ge, where TA, LA and TO phonons have been found to contribute with energies $TA_{Ge\text{-}Ge}$ ~8 meV, $LA_{Ge\text{-}Ge}$ ~28 meV and $TO_{Ge\text{-}Ge}$ = 34.5 meV at a lattice temperature of 4.2 K [43]. We tentatively assign our peak separation to LA phonons in our Sn-rich quantum wells. Finally, the fact that two peaks suffice to fit the PL spectra strengthens the assumption that the overgrowth with Ge has resulted in a flattening of the Sn surface and the disappearance of the islands.

PL spectra obtained at constant lattice temperature but with different excitation power densities are shown in Fig. 4 d). Here, the peak positions show weak variations with excitation density (Fig. 4 e)), and there is no clear trend in the variation of peak position with varying excitation power density. Such behavior has been observed previously [26] and can be indicative of a type-I quantum well structure. Again, we observe an approximately constant peak separation (Fig. 4 f)), although with less overlap in the error bars compared to the temperature-dependent PL analysis. While the slight trend towards increasing separation with increasing excitation power density merits further investigation, we nonetheless take our results as further confirmation that the peaks can be assigned to a phonon-assisted transition and a no phonon-assisted transition, indicating that we have an indirect transition in the material.

The areas under the phonon-assisted and the NP peaks as a function of the inverse lattice temperature and the excitation power density have also been investigated (Fig. 5). A semi-logarithmic plot of integrated PL intensities I of the respective peaks as a function of inverse lattice temperature is shown in Fig. 5 a) together with Arrhenius fits to the data using [44].

$$I(T) = \frac{I_0}{1 + A\exp\left(-\frac{E_a}{k_B T}\right)}, \tag{1}$$

where I_0 is the integrated PL intensity at the lowest measurement temperature, A is a constant and E_a is the thermal activation energy. The extracted thermal activation energies (E_a^{NP} = 8 meV for the NP peak and E_a^{PA} = 23 meV for the phonon-assisted transition) are indicative of thermally activated nonradiative recombination mechanisms. One possible candidate is thermal emission of the carriers out of the quantum

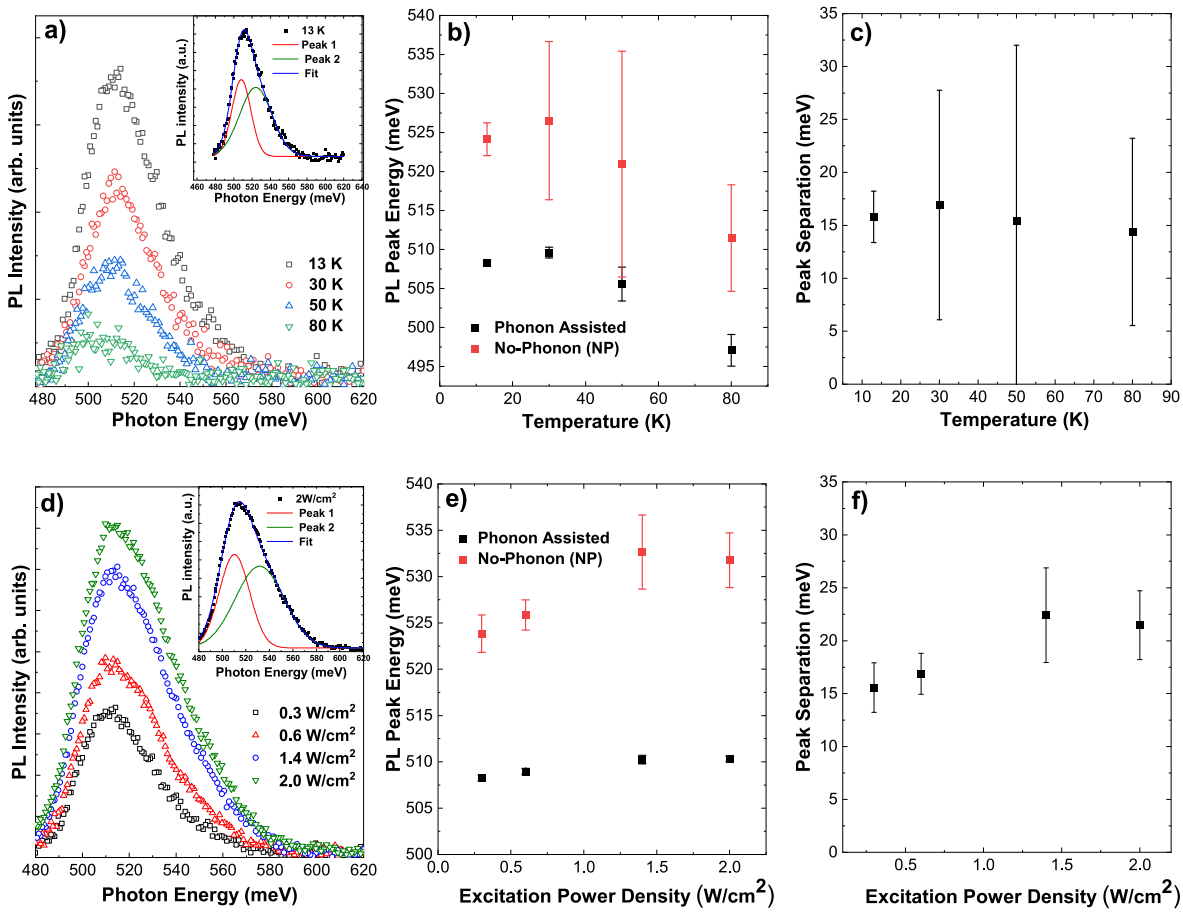

Fig. 4. a) Experimentally observed PL spectra at excitation power densities 0.3 W/cm^2 for different lattice temperatures. All spectra can be fit by two Gaussian peaks, a representative fit is shown in the inset. b) Peak energies extracted from these fits decrease as a function of temperature, while their separation c) is approximately constant. d) The experimentally observed PL spectra at a lattice temperature of 15 K for different excitation power densities can be fit with two Gaussian peaks as shown in the inset. Both the peak energies e) and their separation f) remain approximately constant as a function of excitation power density within the error bars obtained from fitting.

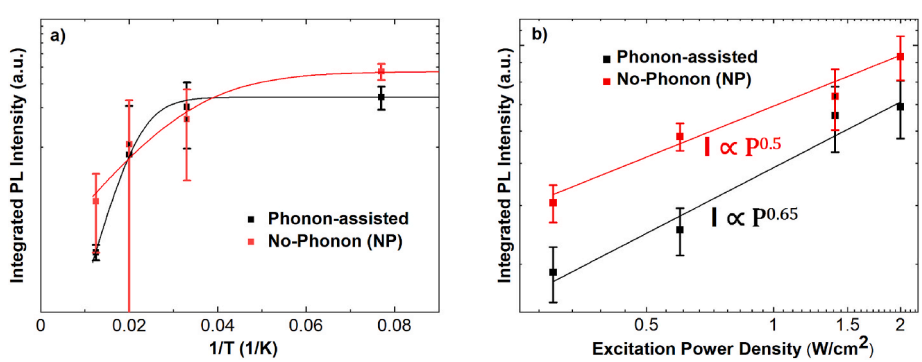

Fig. 5. a) Semi-logarithmic plot of the integrated PL intensities of the phonon-assisted and NP peaks as a function of inverse lattice temperature together with results from Arrhenius fits. b) A power-law relation can be found between the integrated PL intensities and the excitation power density whose exponent points towards Auger recombination as the dominant non-radiative recombination channel.

well, in which case the thermal activation energy is related to the difference in energy between the ground state energy level of the well and non-radiative recombination centers in the vicinity. However, the thermal activation energies extracted for our samples are very low, which either indicates poor confinement or a different dominant non-radiative recombination channel. In our case, the integrated PL intensity shows a power-law dependence on the excitation power density P, i.e. $I \propto P^{\alpha}$, with an exponent $\alpha \sim 0.5$ (Fig. 5 b)) – this points towards Auger recombination as the dominant non-radiative recombination channel. While Auger recombination typically dominates for high excitation power densities, our quantum wells are extremely thin, which can result in high charge carrier densities in our samples.

4. Conclusion

Sn-rich quantum wells and quantum islands are of large interest for applications in optoelectronic devices. The strengths of MBE as a deposition method can be used for the growth of such structures by

depositing few MLs of pure Sn on Ge (001) and overgrowing them with a Ge cap layer. However, obtaining direct optical transitions in these structures is challenging as a result of the low effective electron mass along the confinement direction if the thickness of the Sn-rich region in growth direction is low. Here, we explore a growth regime that utilizes both a low substrate temperature (60 °C) and a low Sn deposition rate ($r_{Sn} = 0.013$ Å/s) and show that, compared to a previous investigation, a higher wetting layer thickness of ~4 ML (compared to 2.25 ML found previously) can be reached before the onset of Sn island formation occurs.

A morphological investigation of uncapped and capped samples containing 4.4 ML and 7.4 ML of Sn indicates that inverse Stranski-Krastanov growth during overgrowth of the sample containing 4.4 ML of Sn flattens the dots, leading to the formation of a Sn-rich quantum well in the capped sample. Overgrowth of the Sn islands with much larger heights in the sample containing 7.4 ML of Sn results in epitaxial breakdown on top of the islands, indicating that there is a limit to material relaxation within the island when overgrowth with crystalline Ge is targeted.

Photoluminescence spectra obtained from the capped sample containing 4.4 ML of Sn can be decomposed into two Gaussian peaks that can be attributed to a phonon-assisted and a no-phonon transition, indicating that transitions remain indirect in our samples. Our investigation nonetheless shows that a careful adjustment of substrate temperature and Sn deposition rate can have a strong influence on the critical layer thickness that marks the onset of island growth. Future investigations should, thus, be targeted at further adjusting this critical layer thickness but also at inducing (partial) relaxation, since material strain has a strong influence on the relative position of the conduction band edges [7,8]. One possible strategy is to target relaxation via nanostructuring e.g. of metasurfaces consisting of nanopillars [26], which, at the same time, can be used to tailor optoelectronic properties. However, our results already indicate that Sn-rich island growth results in a considerable degree of material relaxation within the islands. Thus, using these results as a starting point for a detailed investigation of not only the controlled growth but also the overgrowth of Sn-rich islands is an interesting target of future research efforts both for increasing the thickness of the Sn-rich region and inducing (partial) material relaxation within the islands. Such layers containing optically active material with reduced dimensionality have met with considerable success for III-V quantum dot lasers, leading to increased operating temperature and decreased threshold current densities compared to bulk or quantum well active layers. Our results, thus, constitute an important step towards the fabrication of Sn-rich nanostructures based on MBE growth.

Author statement

Ahsan Hayat: data curation, formal analysis, investigation, writing – original draft, writing-review and editing. Davide Spirito: methodology, data curation, writing – review and editing. Agnieszka Anna Corley-Wiciak: investigation, data curation. Markus Andreas Schubert: investigation, data curation. Maria Masood: investigation, data curation. Felix Reichmann: methodology, validation. Markus Ratzke: data curation, formal analysis. Giovanni Capellini: methodology, formal analysis, writing – review and editing. Inga Anita Fischer: conceptualization, formal analysis, investigation, methodology, supervision, writing – review and editing.

Declaration of competing interest

The authors declare that they have no known competing financial interests or personal relationships that could have appeared to influence the work reported in this paper.

Data availability

Data will be made available on request.

References

[1] I.A. Fischer, M. Brehm, M. De Seta, G. Isella, D.J. Paul, M. Virgilio, G. Capellini, On-chip infrared photonics with Si-Ge-heterostructures: what is next? APL Photonics 7 (2022), 050901.

[2] S. Lischke, et al., Ultra-fast germanium photodiode with 3-DB bandwidth of 265 GHz, Nat. Photonics 15 (2021) 12.

[3] F. Boeuf, et al., Silicon photonics R&d; manufacturing on 300-mm wafer platform, J. Lightwave Technol. 34 (2016) 286.

[4] O. Moutanabbir, et al., Monolithic infrared silicon photonics: the rise of (Si)GeSn semiconductors, Appl. Phys. Lett. 118 (2021), 110502.

[5] D. Buca, et al., Room temperature lasing in GeSn microdisks enabled by strain engineering, Adv. Opt. Mater. 10 (2022), 2201024.

[6] B. Marzban, et al., Strain Engineered Electrically Pumped SiGeSn Microring Lasers on Si, ACS Photonics, 2022.

[7] L. Jiang, J.D. Gallagher, C.L. Senaratne, T. Aoki, J. Mathews, J. Kouvetakis, J. Menéndez, Compositional dependence of the direct and indirect band gaps in Ge 1− y Sn y alloys from room temperature photoluminescence: implications for the indirect to direct gap crossover in intrinsic and n -type materials, Semicond. Sci. Technol. 29 (2014), 115028.

[8] A.A. Tonkikh, C. Eisenschmidt, V.G. Talalaev, N.D. Zakharov, J. Schilling, G. Schmidt, P. Werner, Pseudomorphic GeSn/Ge(001) quantum wells: examining indirect band gap bowing, Appl. Phys. Lett. 103 (2013), 032106.

[9] C.D. Thurmond, F.A. Trumbore, M. Kowalchik, Germanium solidus curves, J. Chem. Phys. 25 (1956) 799.

[10] P. Zaumseil, Y. Hou, M.A. Schubert, N. von den Driesch, D. Stange, D. Rainko, M. Virgilio, D. Buca, G. Capellini, The thermal stability of epitaxial GeSn layers, Apl. Mater. 6 (2018), 076108.

[11] G.-E. Chang, W.-Y. Hsieh, J.-Z. Chen, H.H. Cheng, Quantum-confined photoluminescence from $Ge_{1-x}Sn_x$/Ge superlattices on Ge-buffered Si(001) substrates, Opt. Lett. 38 (2013) 3485.

[12] J.-Z. Chen, H. Li, H.H. Cheng, G.-E. Chang, Structural and optical characteristics of Ge_{1-x}Snx/Ge superlattices grown on Ge-buffered Si(001) wafers, Opt. Mater. Express 4 (2014) 1178.

[13] S. Zhang, S. Shibayama, O. Nakatsuka, Crystalline and optoelectronic properties of Ge1−xSnx/high-Si-Content-SiyGe1−x−ySnx double-quantum wells grown with low-temperature molecular beam epitaxy, Semicond. Sci. Technol. 38 (2022), 015018.

[14] W. Dondl, P. Schittenhelm, G. Abstreiter, Self-assembled growth of Sn on Ge (001), Thin Solid Films 294 (1997) 308.

[15] Y. Nakamura, A. Masada, S.-P. Cho, N. Tanaka, M. Ichikawa, Epitaxial growth of ultrahigh density Ge1−xSnx quantum dots on Si (111) substrates by codeposition of Ge and Sn on ultrathin SiO2 films, J. Appl. Phys. 102 (2007), 124302.

[16] R. Ragan, K.S. Min, H.A. Atwater, Direct energy gap group IV semiconductor alloys and quantum dot arrays in SnxGe1−x/Ge and SnxSi1−x/Si alloy systems, Mater. Sci. Eng. B 87 (2001) 204.

[17] F. Oliveira, I.A. Fischer, A. Benedetti, M.F. Cerqueira, M.I. Vasilevskiy, S. Stefanov, S. Chiussi, J. Schulze, Multi-stacks of epitaxial GeSn self-assembled dots in Si: structural analysis, J. Appl. Phys. 117 (2015), 125706.

[18] F. Oliveira, I.A. Fischer, A. Benedetti, P. Zaumseil, M.F. Cerqueira, M.I. Vasilevskiy, S. Stefanov, S. Chiussi, J. Schulze, Fabrication of GeSn-multiple quantum wells by overgrowth of Sn on Ge by using molecular beam epitaxy, Appl. Phys. Lett. 107 (2015), 262102.

[19] I.A. Fischer, et al., Growth and characterization of SiGeSn quantum well photodiodes, Opt Express 23 (2015), 25048.

[20] B. Schwartz, et al., Electroluminescence of GeSn/Ge MQW LEDs on Si substrate, Opt. Lett. 40 (2015) 3209.

[21] D. Stange, et al., Short-wave infrared LEDs from GeSn/siGeSn multiple quantum wells, Optica 4 (2017) 185.

[22] W. Wegscheider, K. Eberl, U. Menczigar, G. Abstreiter, Single-crystal Sn/Ge superlattices on Ge substrates: growth and structural properties, Appl. Phys. Lett. 57 (1990) 875.

[23] K. Eberl, W. Wegscheider, G. Abstreiter, Group IV element (Si, Ge and α-Sn) superlattices — low temperature MBE, J. Cryst. Growth 111 (1991) 882.

[24] W. Wegscheider, J. Olajos, U. Menczigar, W. Dondl, G. Abstreiter, Fabrication and properties of epitaxially stabilized Ge/α-Sn heterostructures on Ge(001), J. Cryst. Growth 123 (1992) 75.

[25] P. Vogl, J. Olajos, W. Wegscheider, G. Abstreiter, Electronic structure and optical properties of short-period α-SnnGem superlattices, Surf. Sci. 267 (1992) 83.

[26] I.A. Fischer, et al., Composition analysis and transition energies of ultrathin Sn-rich GeSn quantum wells, Phys. Rev. Mater. 4 (2020), 024601.

[27] Y.-W. Mo, D.E. Savage, B.S. Swartzentruber, M.G. Lagally, Kinetic pathway in stranski-krastanov growth of Ge on Si(001), Phys. Rev. Lett. 65 (1990) 1020.

[28] F. Oliveira, I.A. Fischer, A. Benedetti, P. Zaumseil, M.F. Cerqueira, M.I. Vasilevskiy, S. Stefanov, S. Chiussi, J. Schulze, Fabrication of GeSn-multiple quantum wells by overgrowth of Sn on Ge by using molecular beam epitaxy, Appl. Phys. Lett. 107 (2015), 262102.

[29] E.V.S. Hofmann, E. Scalise, F. Montalenti, T.J.Z. Stock, S.R. Schofield, G. Capellini, L. Miglio, N.J. Curson, W.M. Klesse, The Formation of a Sn monolayer on Ge(100) studied at the atomic scale, Appl. Surf. Sci. 561 (2021), 149961.

[30] O. Skibitzki, et al., Reduction of threading dislocation density beyond the saturation limit by optimized reverse grading, Phys. Rev. Mater. 4 (2020), 103403.
[31] G. Capellini, M. De Seta, F. Evangelisti, Ge/Si(100) islands: growth dynamics versus growth rate, J. Appl. Phys. 93 (2003) 291.
[32] A. Rastelli, M. Kummer, H. von Känel, Reversible shape evolution of Ge islands on Si(001), Phys. Rev. Lett. 87 (2001), 256101.
[33] M. Stoffel, G.S. Kar, U. Denker, A. Rastelli, H. Sigg, O.G. Schmidt, Shape, facet evolution and photoluminescence of Ge islands capped with Si at different temperatures, Phys. E Low-Dimens. Syst. Nanostructures 23 (2004) 421.
[34] G. Capellini, M. De Seta, L. Di Gaspare, F. Evangelisti, F. d'Acapito, Evolution of Ge/Si(001) islands during Si capping at high temperature, J. Appl. Phys. 98 (2005), 124901.
[35] A. Bernardi, M.I. Alonso, J.S. Reparaz, A.R. Goñi, P.D. Lacharmoise, J.O. Ossó, M. Garriga, Evolution of strain and composition during growth and capping of Ge quantum dots with different morphologies, Nanotechnology 18 (2007), 475401.
[36] M. Brehm, M. Grydlik, H. Groiss, F. Hackl, F. Schäffler, T. Fromherz, G. Bauer, The influence of a Si cap on self-organized SiGe islands and the underlying wetting layer, J. Appl. Phys. 109 (2011), 123505.
[37] C.W. Petz, J.A. Floro, Inhomogeneous low temperature epitaxial breakdown during Si overgrowth of GeSi quantum dots, J. Appl. Phys. 110 (2011), 023508.
[38] J. Cui, Q. He, X.M. Jiang, Y.L. Fan, X.J. Yang, F. Xue, Z.M. Jiang, Self-assembled SiGe quantum rings grown on Si(001) by molecular beam epitaxy, Appl. Phys. Lett. 83 (2003) 2907.
[39] S. Christiansen, M. Albrecht, H.P. Strunk, P.O. Hansson, E. Bauser, Reduced effective misfit in laterally limited structures such as epitaxial islands, Appl. Phys. Lett. 66 (1995) 574.
[40] C.-P. Liu, Evolution of Ge/Si(001) islands upon oxidation and water etching, Thin Solid Films 415 (2002) 296.
[41] G. Capellini, M. De Seta, F. Evangelisti, C. Spinella, Strain relief mechanisms in Ge/Si(100) islands, Mater. Sci. Eng. B 101 (2003) 106.
[42] E. Kasper, M. Kittler, M. Oehme, T. Arguirov, Germanium tin: silicon photonics toward the mid-infrared [invited], Photon. Res. 1 (2013) 69.
[43] J. Weber, M.I. Alonso, Near-band-gap photoluminescence of Si-Ge alloys, Phys. Rev. B 40 (1989) 5683.
[44] J.D. Lambkin, D.J. Dunstan, K.P. Homewood, L.K. Howard, M.T. Emeny, Thermal quenching of the photoluminescence of InGaAs/GaAs and InGaAs/AlGaAs strained-layer quantum wells, Appl. Phys. Lett. 57 (1990) 1986.